Supplementary Data

Supplementary Data contains Supplementary Methods, Supplementary References, five Supplementary Figures and eight Supplementary Tables.

Supplementary Methods

Cell culture

Madin Darby canine kidney (MDCK) cell lines (ATCC; CCL-34) were routinely cultured in complete medium (DMEM-C), containing DMEM GlutaMAX™, supplemented with 10% FBS, penicillin (50 U/ml), streptomycin (50 µg/ml). Human alveolar adenocarcinoma (A549) cells (ATCC; CCL-185), wildtype Chinese hamster ovary (CHO-K1) cells and its ether lipid-deficient variant NRel-4 (both cell lines kindly provided by Raphael A. Zoeller (Boston University, USA) were cultured in Ham's F12 GlutaMAX™ complete medium (Ham's F12-C), supplemented with 10% FBS, penicillin (50 U/ml), streptomycin (50 µg/ml). The cells were incubated at 5% CO_2, 37°C with 80-95% relative humidity. All culture medium reagents were purchased from Gibco®, Life Technologies Co. (San Diego, California, USA).

Virus purification

Egg-grown influenza virus A/PR/8/34 H1N1 was kindly provided by Mike Kemeney (Department of Microbiology, National University of Singapore); egg-grown human influenza virus strain A/Aichi/2/68 H3N2 P0 and egg-grown mouse-adapted human influenza virus strain A/Aichi/2/68 H3N2 P10 were kindly provided by Vincent Chow (Department of Microbiology, NUS). Cells were grown to 80-100% confluency and infected with influenza virus (influenza virus A/PR/8/34 H1N1, influenza virus A/Aichi/2/68 H3N2 P0 or influenza

virus A/Aichi/2/68 H3N2 P10) in MDCK-infection medium (serum-free DMEM-C supplemented with TPCK trypsin (2 µg/ml; Sigma-Aldrich, St. Louis, USA)) or A549-infection medium (serum-free Ham's F12-C with TPCK trypsin (1 µg/ml)). The inoculum was exchanged after 1 hour with fresh serum-free complete medium. The supernatant was collected after 48 to 72 hours post-infection (hpi). The viruses were purified as previously described (42). The virus supernatant was clarified twice by centrifugation for ten minutes in a pre-chilled bench top centrifuge at 4000 rpm (4^{o}C) (Eppendorf, Hamburg, Germany). The clarified supernatant was subsequently layered over 20% sucrose cushions dissolved in 1× phosphate-buffered saline (PBS) and concentrated by ultracentrifugation at 112,600 ×g for 2 hours at 4°C . Virus pellets were dissolved in 1× PBS and carefully dislodged overnight at 4°C before layering the concentrated virus over 30% to 60% sucrose gradients (seven steps). The gradient was centrifuged at 112,600 ×g for 3 hours at 4°C and the banded virus (1.18 g/cm^3 to 1.19 g/cm^3; interface between 40% and 45% sucrose) was carefully collected, combined and diluted with 1× PBS. Finally, purified influenza viruses were pelleted by centrifugation at 112,600 ×g for 2 hours at 4°C and the pellet was carefully dislodged in 1× PBS overnight at 4°C after aspirating the supernatant. Virus titres were determined by plaque assay as previously described (43). Virus purity was assessed by SDS-PAGE and coomassie blue staining, and initial SEM pictures were taken from negative-stained purified MDCK-grown influenza virus A/Aichi/2/68 H3N2 P10 virus particles (Figure S1B). For all experiments, viruses were not grown for more than three passages in any given cell line.

Lipid extraction

Lipids were extracted using a modified Bligh and Dyer protocol (44). Only pre-chilled HPLC grade reagents were used. The cells were harvested at the respective timepoints by washing twice with ice-cold 1×PBS and then scraped in 500 µl ice-cold methanol and transferred into

fresh tubes. 250 µl of chloroform was then added to the mixture to adjust the ratio of chloroform:methanol to 1:2. For purified influenza viruses, 150 µl of virus preparations were split into 50 µl aliquots for independent extraction, and chloroform:methanol (1:2, v/v) was added directly. The mixtures were incubated and extracted as previously described (20, 21). Samples were dried under vacuum using a miVac Duo Concentrator (Genevac Ltd, Suffolk, UK) and were stored at -80°C until further analysis by high performance liquid chromatograph-mass spectrometry (HPLC MS).

Internal standards for high performance liquid chromatography mass spectrometry (HPLC MS/MS) analyses

Synthetic lipid standards were spiked to the lipid extracts post-extraction prior to HPLC MS analyses. Specifically, the following standards were included for PS (dimyristoyl-phosphatidylserine or DMPS; final concentration 2µg/ml), PE (dimyristoyl-phosphatidylethanolamine or DMPE; final concentration 10µg/ml), PI (dioctanoyl-phosphatidylinositol or C8PI; final concentration 1µg/ml), PC (dimyristoyl-phosphatidylcholine or DMPC; final concentration 10µg/ml), SM (lauroyl sphingomyelin or LSM; final concentration 2µg/ml), Cer (N-heptadecanoyl-D-erythro-sphingosine or C17Cer; final concentration 1µg/ml), HexCer (D-glucosyl-ß1-1'-N-octanoyl-D-erythro-sphingosine or C8HexCer; final concentration 1µg/ml), TAG (d5-TAG 48:0 (5µg/ml)), cholesterol ester (d6-C18 cholesterol ester (10µg/ml)), DAG (4-methyl 16:0 diether DAG (3µg/ml)) and cholesterol (d6-cholesterol (5µg/ml)). Glycerophospho- and sphingolipid standards were purchased from Avanti Polar Lipids, Inc. (Alabama, USA). Internal standards for TAG, cholesterol ester and cholesterol were obtained from C/D/N Isotopes Inc. (Quebec, Canada).

Quantitative analysis of lipids by HPLC MS/MS

For glycerophospho- and sphingolipid analyses, dried cellular and viral lipid extracts were reconstituted in 60 to 80 µl of chloroform:methanol (1:1 v/v). The samples were spiked with internal standards and 15 µl of the sample-standard mixture was injected using an Agilent 1200 Thermo Sampler (Agilent, California, USA). Lipid classes were separated by HPLC using a Luna 3-µm silica column (Phenomenex Inc, California, USA) coupled to an Agilent 1200 HPLC system (Agilent, California, USA). Lipids were analysed by a targeted multiple reaction monitoring (MRM) of 159 unique transitions (Table S2) using a triple quadrupole instrument ABI 3200 QT (Applied Biosystems, California, USA) as previously described (20, 21). Using this HPLC separation method, 16 odd chain PC species were distinguished from ePC species by their different elution time. Note, that we cannot exclude methyl-branching of fatty acyls from odd chain fatty acyls using these methods. Furthermore, sphingosine (d18:1) and sphinganine (d18:0) containing SM species were also separated based on their elution time. For neutral lipid analyses, the sample-standard mixture (30 µl) was injected and neutral lipids (DAG and TAG species, cholesterol ester and cholesterol) were analysed by reverse phase HPLC/ESI/MS on an ABI 3200QT (Applied Biosystems, Foster City CA) instrument coupled to an Agilent 1200 HPLC system (Agilent, California, USA) as previously described (21, 45, 46). Eighty-four ions were monitored in the positive ion mode.

Analysis of MS raw data

Signal intensities for each lipid species were extracted according to their retention time and imported into Microsoft Excel (Microsoft, Washington, USA). Concentrations of measured lipid species were calculated by normalisation to the representative spiked internal standards, with the exception of GM3 levels, which were normalised to the PI internal standard (C8PI). Lipid species were represented as a molar fraction of the total amount of measured lipid

species (20). Data were represented either as heatplots of ratios between two different conditions or by basic bar plots with standard deviations drawn in Microsoft Excel. Statistical significance was calculated using an unpaired student's t-test ($p<0.05$; two-tailed) except for the identification of significantly altered lipid species in A549 cells. To control for batch variations of independent mass spectrometry runs (the three independent experiments were independently analysed by mass spectrometry over an extended period of time), a block-design three-way (batch, infection, time point) ANOVA was performed and multiple tests were corrected for by a false discovery rate (FDR) procedure, using functions aov and p.adjust, respectively, in the R package "stats" (47). Only later time points (18hpi and 24hpi) were considered and FDR ($q<0.006$) represented a significant difference at 18 and/or 24hpi. Fold-changes of lipid species were correlated to virus titres at 12, 18 and 24hpi, and the cumulative distribution of calculated Pearson's correlation coefficients was plotted in Microsoft Excel.

Hierarchical clustering of lipid species

The MRM data from eight independent experiments describing host response (virus-induced changes in A549 cells at 18hpi and 24hpi; three independent experiments; Table S2), viral lipids (the lipid profile of influenza virus A/PR/8/34 H1N1 compared to its A549 producer cell; 2 independent experiments; Table S3) and virulence (differences between influenza virus A/Aichi/2/68 H3N2 P0 and P10 strains; 3 independent experiments; Table S5) were considered for clustering of fold ratios (Table S8). Lipid species with missing values were excluded which resulted in a list of 146 lipid species (Table S6). Prior to hierarchical clustering, the data was rescaled to obtain 1 or -1 as the maximum change for each lipid species. Subsequently, lipids were clustered using Pearson correlation distances (uncentered) with average-linkage implemented in the open source clustering software Cluster 3.0 (48).

Since there are 2^{N-1} (2145) ordering consistent with any tree of N (146) items (lipid species), a GORDER value consistent with the order of the input data was assigned. The input data was sorted according to lipid classes (PS, PI, GM3, aPE, ePE, aPC, ePC, SM, Cer, HexCer) followed by saturation and chain length and the assigned GORDER values increased for each lipid species based on its position in the list order (1 to 146). This ensured that the lipid order produced by clustering was as close as possible (without violating the structure of the dendrogram) to the original lipid order. The calculated dendrogram was visualised using the open source software Java TreeView (49) with the colours red (upregulation), blue (downregulation) and white (no change). Approximately unbiased p-values were estimated using multiscale bootstrap resampling (n=10,000) by the pvclust package implemented in R (47, 50). Patterns in 13 identified clusters were further analysed by plotting the average change for each lipid species and the average change for the whole clusters with standard deviations in Microsoft Excel. Correlations of 13 clusters with virus titre were plotted as medians depicted with Q_1, Q_3 and 1.5*inter quartile range (IQR) using the boxplot function in R (47).

Knockdown of AGPS and Rab11a by siRNA

Reverse transfection of siRNA constructs into A549 cells using Lipofectamine RNAiMAX (Invitrogen®, Life Technologies Co. (San Diego, California, USA) was performed according to the manufacturer's protocol. Three different concentrations (3 nM, 6 nM and 12 nM) were used and for each experiment, with two replicates of water and scrambled siRNA controls performed. Cells were collected after 48 hours post-transfection. Knockdown efficiency was assessed by reverse transcription quantitative polymerase chain reaction (RT-qPCR) and western blot. Antibodies against Rab11a (Abcam, Cambridge, UK) and AGPS (Sigma-Aldrich, St. Louis, USA) were used in combination with anti-GAPDH and anti-α-tubulin

antibodies as loading controls. The degree of ether lipid depletion was measured by mass spectrometry as described above. For virus infection experiments, siRNA-transfected cells grown for 48 hours were infected with influenza virus A/PR/8/34 H1N1 (MOI <1). Cell lysates and virus supernatants were collected after an additional incubation for 18 hours and subjected to western blot and plaque assay. Significant differences were calculated by an unpaired student's t-test ($p<0.05$; two-tailed).

Literature mining

ePC/aPC ratios of purified viruses were compared with their uninfected producer cells, calculating $\Delta_{Virus\text{-}Cell}$=ePC/aPC$_{Virus}$-ePC/aPC$_{Cell}$. Statistically significant differences between influenza viruses and other enveloped viruses (9, 20, 51-54) were calculated based on the $\Delta_{Virus\text{-}Cell}$ values by an unpaired student's t-test ($p<0.05$; two-tailed). We reanalysed 458 previously described susceptibility factors to influenza virus infection (39). Twenty-three lipid-associated genes were manually annotated to KEGG pathways (55, 56) or by DAVID (57, 58). Significant enrichment was calculated by an uncorrected and Benjamini-corrected EASE score ($p<0.05$). (3-5, 22, 59-61), proteomics (6-8), metabolomics (15, 19) and cell biological data (11, 14, 62-65) (Table S7).

Supplementary References

42. Shaw, M. L., K. L. Stone, C. M. Colangelo, E. E. Gulcicek, and P. Palese. 2008. Cellular proteins in influenza virus particles. *PLoS pathogens* **4**: e1000085.

43. Matrosovich, M., T. Matrosovich, W. Garten, and H. D. Klenk. 2006. New low-viscosity overlay medium for viral plaque assays. *Virology journal* **3**: 63.

44. Bligh, E. G., and W. J. Dyer. 1959. A rapid method of total lipid extraction and purification. *Canadian journal of biochemistry and physiology* **37**: 911-917.

45. Shui, G., X. L. Guan, C. P. Low, G. H. Chua, J. S. Goh, H. Yang, and M. R. Wenk. 2010. Toward one step analysis of cellular lipidomes using liquid chromatography coupled with mass spectrometry: application to Saccharomyces cerevisiae and Schizosaccharomyces pombe lipidomics. *Molecular bioSystems* **6**: 1008-1017.

46. Tan, S. H., G. Shui, J. Zhou, J. J. Li, B. H. Bay, M. R. Wenk, and H. M. Shen. 2012. Induction of autophagy by palmitic acid via protein kinase C-mediated signaling pathway independent of mTOR (mammalian target of rapamycin). *The Journal of biological chemistry* **287**: 14364-14376.

47. R Development Core Team. 2010. R: A language and environment for statistical computing. *In*. R Foundation for Statistical Computing, Vienna, Austria.

48. de Hoon, M. J., Y. Makita, S. Imoto, K. Kobayashi, N. Ogasawara, K. Nakai, and S. Miyano. 2004. Predicting gene regulation by sigma factors in Bacillus subtilis from genome-wide data. *Bioinformatics* **20 Suppl 1**: i101-108.

49. Saldanha, A. J. 2004. Java Treeview--extensible visualization of microarray data. *Bioinformatics* **20**: 3246-3248.

50. Suzuki, R., and H. Shimodaira. 2006. Pvclust: an R package for assessing the uncertainty in hierarchical clustering. *Bioinformatics* **22**: 1540-1542.

51. Kalvodova, L., J. L. Sampaio, S. Cordo, C. S. Ejsing, A. Shevchenko, and K. Simons. 2009. The lipidomes of vesicular stomatitis virus, semliki forest virus, and the host plasma membrane analyzed by quantitative shotgun mass spectrometry. *Journal of virology* **83**: 7996-8003.

52. Lorizate, M., T. Sachsenheimer, B. Glass, A. Habermann, M. J. Gerl, H. G. Krausslich, and B. Brugger. 2013. Comparative lipidomics analysis of HIV-1 particles and their producer cell membrane in different cell lines. *Cellular microbiology* **15**: 292-304.

53. Merz, A., G. Long, M. S. Hiet, B. Brugger, P. Chlanda, P. Andre, F. Wieland, J. Krijnse-Locker, and R. Bartenschlager. 2011. Biochemical and morphological properties of hepatitis C virus particles and determination of their lipidome. *The Journal of biological chemistry* **286**: 3018-3032.

54. Zhang, Q., C. Hunke, Y. H. Yau, V. Seow, S. Lee, L. B. Tanner, X. L. Guan, M. R. Wenk, G. Fibriansah, P. L. Chew, P. Kukkaro, G. Biukovic, P. Y. Shi, S. G. Shochat, G. Gruber, and S. M. Lok. 2012. The stem region of premembrane protein plays an important role in the virus surface protein rearrangement during dengue maturation. *The Journal of biological chemistry* **287**: 40525-40534.

55. Kanehisa, M., and S. Goto. 2000. KEGG: kyoto encyclopedia of genes and genomes. *Nucleic acids research* **28**: 27-30.

56. Kanehisa, M., S. Goto, Y. Sato, M. Furumichi, and M. Tanabe. 2012. KEGG for integration and interpretation of large-scale molecular data sets. *Nucleic acids research* **40**: D109-114.

57. Huang da, W., B. T. Sherman, and R. A. Lempicki. 2009. Systematic and integrative analysis of large gene lists using DAVID bioinformatics resources. *Nature protocols* **4**: 44-57.

58. Huang da, W., B. T. Sherman, and R. A. Lempicki. 2009. Bioinformatics enrichment tools: paths toward the comprehensive functional analysis of large gene lists. *Nucleic acids research* **37**: 1-13.

59. Sui, B., D. Bamba, K. Weng, H. Ung, S. Chang, J. Van Dyke, M. Goldblatt, R. Duan, M. S. Kinch, and W. B. Li. 2009. The use of Random Homozygous Gene Perturbation to identify novel host-oriented targets for influenza. *Virology* **387**: 473-481.

60. Watanabe, T., S. Watanabe, and Y. Kawaoka. 2010. Cellular networks involved in the influenza virus life cycle. *Cell host & microbe* **7**: 427-439.

61. Geiss, G. K., M. Salvatore, T. M. Tumpey, V. S. Carter, X. Wang, C. F. Basler, J. K. Taubenberger, R. E. Bumgarner, P. Palese, M. G. Katze, and A. Garcia-Sastre. 2002. Cellular transcriptional profiling in influenza A virus-infected lung epithelial cells: the role of the nonstructural NS1 protein in the evasion of the host innate defense and its potential contribution to pandemic influenza. *Proceedings of the National Academy of Sciences of the United States of America* **99**: 10736-10741.

62. Ehrhardt, C., and S. Ludwig. 2009. A new player in a deadly game: influenza viruses and the PI3K/Akt signalling pathway. *Cellular microbiology* **11**: 863-871.

63. Ehrhardt, C., T. Wolff, S. Pleschka, O. Planz, W. Beermann, J. G. Bode, M. Schmolke, and S. Ludwig. 2007. Influenza A virus NS1 protein activates the PI3K/Akt pathway to mediate antiapoptotic signaling responses. *Journal of virology* **81**: 3058-3067.

64. Zhirnov, O. P., and H. D. Klenk. 2007. Control of apoptosis in influenza virus-infected cells by up-regulation of Akt and p53 signaling. *Apoptosis : an international journal on programmed cell death* **12**: 1419-1432.

65. Moseley, C. E., R. G. Webster, and J. R. Aldridge. 2010. Peroxisome proliferator-activated receptor and AMP-activated protein kinase agonists protect against lethal influenza virus challenge in mice. *Influenza and other respiratory viruses* **4**: 307-311.

66. Perry, R. J., and N. D. Ridgway. 2004. The role of de novo ceramide synthesis in the mechanism of action of the tricyclic xanthate D609. *Journal of lipid research* **45**: 164-173.

67. Albi, E., and M. P. Viola Magni. 2004. The role of intranuclear lipids. *Biology of the cell / under the auspices of the European Cell Biology Organization* **96**: 657-667.

68. Kitatani, K., J. Idkowiak-Baldys, and Y. A. Hannun. 2008. The sphingolipid salvage pathway in ceramide metabolism and signaling. *Cellular signalling* **20**: 1010-1018.

69. Luberto, C., and Y. A. Hannun. 1998. Sphingomyelin synthase, a potential regulator of intracellular levels of ceramide and diacylglycerol during SV40 transformation. Does sphingomyelin synthase account for the putative phosphatidylcholine-specific phospholipase C? *The Journal of biological chemistry* **273**: 14550-14559.

70. Luberto, C., D. S. Yoo, H. S. Suidan, G. M. Bartoli, and Y. A. Hannun. 2000. Differential effects of sphingomyelin hydrolysis and resynthesis on the activation of NF-kappa B in normal and SV40-transformed human fibroblasts. *The Journal of biological chemistry* **275**: 14760-14766.

Supplementary Figure Legends

Figure S1: Relative molar fraction [%] of lipid classes during influenza virus infection observed in three independent experiments (linked to Figure 1 in the main text). Influenza virus consistently impacts SPL, ePC and oPC lipid classes across three independent experiments. *p<0.05, **p<0.005 (unpaired student's t-test; two-tailed). Data are from three biological replicates per condition in each independent experiment.

Figure S2: Absolute concentration [µg/ml] of lipid classes during influenza virus infection observed in three independent experiments (linked to Figure 1 in the main text). Influenza virus consistently impacts SPL, ePC and oPC lipid classes across three independent experiments. *p<0.05, **p<0.005 (unpaired student's t-test; two-tailed). Data are from three biological replicates per condition in each independent experiment.

Figure S3: Differences between the parent influenza A virus (P0; strain A/Aichi/2/1968 H3N2) and its more virulent mutant P10 strain (linked to Figure 2E in the main text). (A) Fold change in the numbers of significantly different lipid species (p<0.05; unpaired student's t-test; two-tailed). Data are from three independent experiments with two replicates (n=6 per virus strain). **(B)** Absolute concentrations [µg/ml] of ePC and aPC lipids in the two different virus strains. (*p<0.01; unpaired student's t-test; two-tailed). Data are from three independent experiments with two replicates (n=6 per virus strain). **(C)** Scanning electron microscopy picture of purified MDCK-grown H3N2 P10 virus particles.

Figure S4: D609 inhibits a sphingomyelin (SM) salvage pathway (linked to Figure 4A in the main text). (A) Experimental setup to investigate impact of SM synthase (SMS) inhibition by D609 on late stages of influenza virus replication. D609 was added 12 hours post-infection (hpi) and virus titre was assessed by plaque assay 18 hpi. For lipid analysis,

A549 cells were treated with 10 μM D609 for 18 hours in serum free medium. **(B)** Effects of D609 on sphingolipid (SPL) and ether lipid metabolism. Cer, HexCer and ganglioside GM3 species accumulated while SM levels remained unchanged, indicating induction of *de novo* SPL biosynthesis (66). Ether-linked phosphatidylcholine (ePC) species, but not ester-linked phosphatidylcholine (aPC) or other major phospholipids, increased, reflecting a decreased PC-PLC and/or SMS activity since ePC species appeared to be a better substrate than aPC species (67). **(C)** Effects of D609 on *de novo* SPL biosynthesis and SM salvage (resynthesis) pathway. Higher sphinganine (d18:0) to sphingosine (d18:1) ratios were observed in D609 treated cells, further supporting stimulation of *de novo* SPL biosynthesis (68). Specificity towards inhibition of an SM salvage pathway (69, 70) rather than *de novo* SM biosynthesis was reflected by increased levels of sphinganine, but decreased levels of sphingosine containing SM. Data is from one experiment with two (Ctrl) and three (D609) biological replicates ± standard deviations.

Figure S5: ePC content in CHO-K1 cells is elevated but not changed in ether lipid deficient NRel-4 cells upon influenza infection (linked to Figure 4B in the main text). (A) Fold-changes of the 90 altered lipid species identified in A549 cells in comparison to CHO-K1 and NRel-4 cells at 18 hours post-infection (hpi). **(B)** Comparison of lipid classes between H1N1- (light grey bars) and mock-infected (dark grey bars) CHO-K1 and NRel-4 cells. $^{*}p<0.05$ (unpaired student's t-test; two-tailed). **(C)** Comparison of fold-change in the total contents of ePC and GM3, which were significantly altered in A549 cells at 18 hpi. Data in all panels are from one experiment with three replicates (CHO-K1 and NRel-4 cells) and from three experiments with three replicates (A549 cells) for each condition (H1N1 and mock-infected cells) ± standard deviations.

Figure S6: Efficient siRNA knockdown of AGPS (linked to Figure 4C in the main text). **(A)** RT-PCR results of AGPS gene expression upon siRNA knockdown. Data are from three independent experiments with three replicates each ± standard deviations. **(B)** Lipid analysis of A549 cells after siRNA knockdown of AGPS. siRNA and scrambled siRNA control (-ve) cells were grown for 48 hours, and lipids were extracted and analysed as described below. Data are from two independent experiments with three replicates each ± standard deviations. $^{*}p<0.05$, $^{**}p<0.01$, $^{***}p<0.001$ (unpaired student's t-test; two-tailed).

Figure S7: Triacylglycerol (TAG) content in virus-infected cells (linked to the model in Figure 4G in the main text). TAG levels were measured from virus- (light grey bars) and mock-infected (dark grey bars) A549 cells as described below. Data are from two independent experiments with three replicates (n=6 per condition) ± standard deviations. $^{*}p<0.001$, $^{**}p<0.0001$, (unpaired student's t-test; two-tailed).

Supplementary Table Legends:

Table S1: Raw data of influenza virus growth in A549 cells used for Figure 1.

Table S2: Raw data of measured lipid species in influenza virus infected A549 cells at 12, 18 and 24 hours post-infection used for Figure 1.

Table S3: Raw data of measured lipid species in purified influenza virions compared with their A549 producer cells used for Figure 2.

Table S4: Overview of ether-linked phosphatidylcholine to ester-linked phosphatidylcholine (ePC/aPC) ratios in influenza and other enveloped viruses compared with their producer cells used for Figure 2.

Table S5: Raw data of measured lipid species from two influenza virus strains differing in their pathogenicity used for Figure 2.

Table S6: Complete hierarchical clustering results used for Figure 3.

Table S7: Complete list of genes, proteins and metabolites included in the model presented in Figure 4.

Table S8: Overview of experiments and replicates used for lipid analyses.

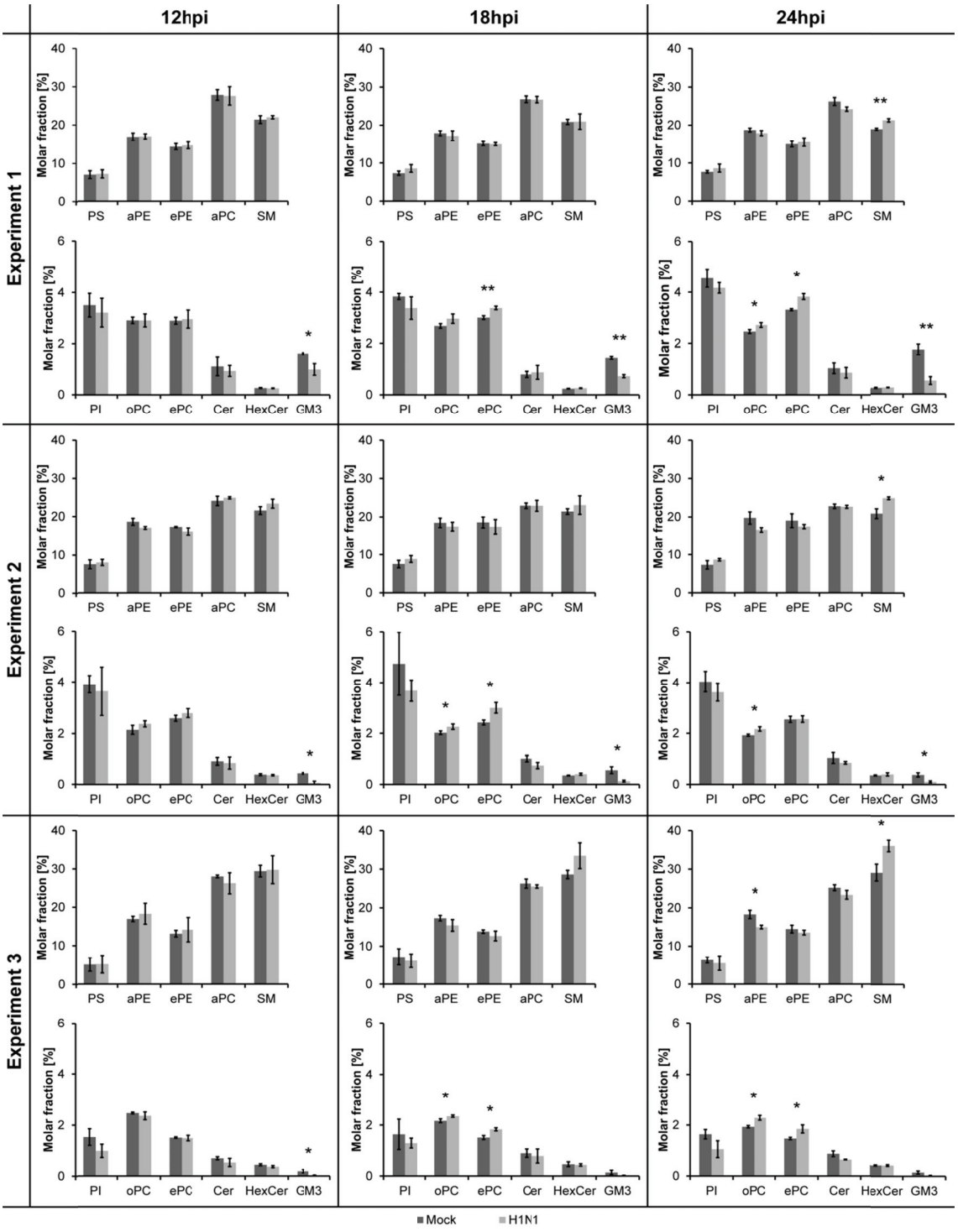
12hpi
18hpi
24hpi
Experiment 1
Experiment 2
Experiment 3
Molar fraction [%]
PS
aPE
ePE
aPC
SM
PI
oPC
ePC
Cer
HexCer
GM3
Mock
H1N1

Figure S1

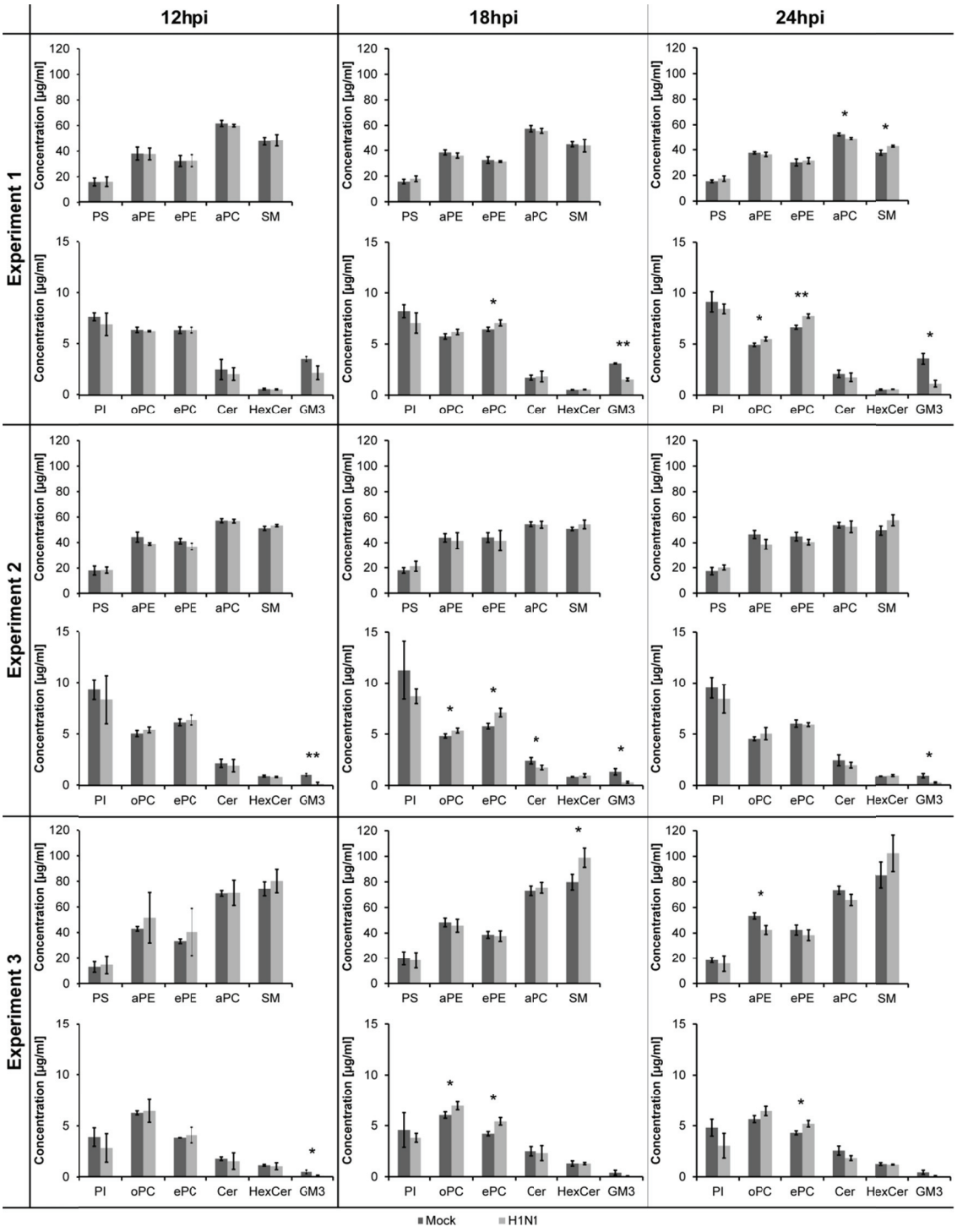
12hpi
18hpi
24hpi
Experiment 1
Experiment 2
Experiment 3
Concentration [µg/ml]
PS
aPE
ePE
aPC
SM
PI
oPC
ePC
Cer
HexCer
GM3
Mock
H1N1

Figure S2

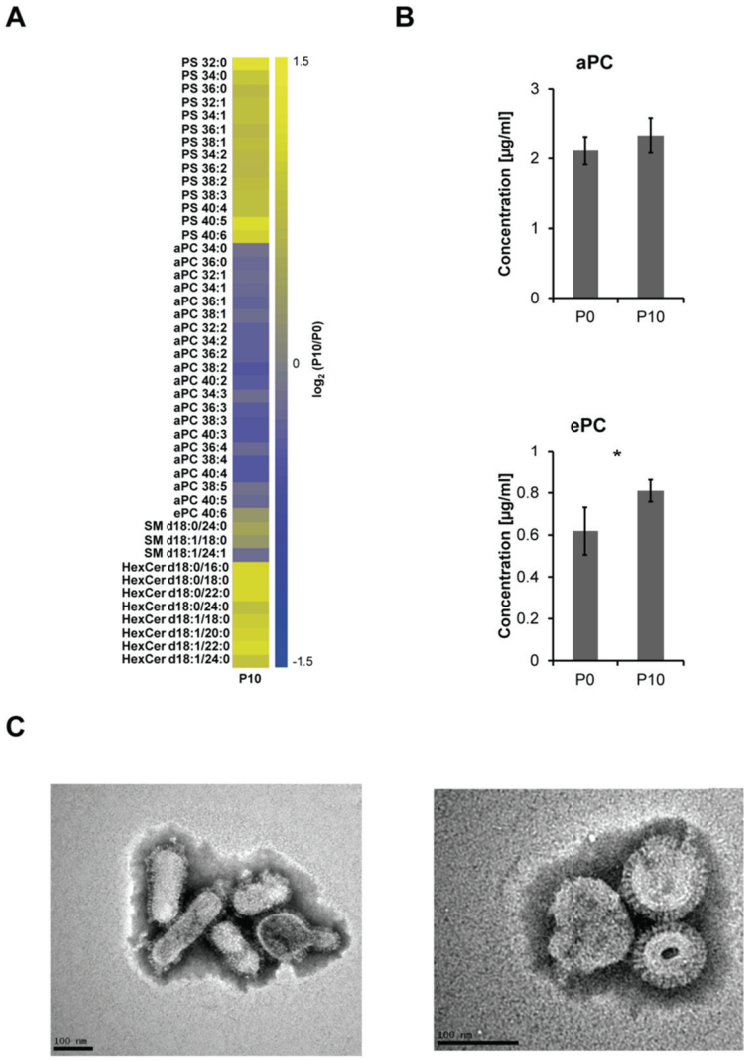
A
B
C
PS 32:0
PS 34:0
PS 36:0
PS 32:1
PS 34:1
PS 36:1
PS 38:1
PS 34:2
PS 36:2
PS 38:2
PS 38:3
PS 40:4
PS 40:5
PS 40:6
aPC 34:0
aPC 36:0
aPC 32:1
aPC 34:1
aPC 36:1
aPC 38:1
aPC 32:2
aPC 34:2
aPC 36:2
aPC 38:2
aPC 40:2
aPC 34:3
aPC 36:3
aPC 38:3
aPC 40:3
aPC 36:4
aPC 38:4
aPC 40:4
aPC 38:5
aPC 40:5
ePC 40:6
SM d18:0/24:0
SM d18:1/18:0
SM d18:1/24:1
HexCer d18:0/16:0
HexCer d18:0/18:0
HexCer d18:0/22:0
HexCer d18:0/24:0
HexCer d18:1/18:0
HexCer d18:1/20:0
HexCer d18:1/22:0
HexCer d18:1/24:0
P10
1.5
0
-1.5
log2 (P10/P0)
aPC
Concentration [µg/ml]
3
2
1
0
P0
P10
ePC
*
Concentration [µg/ml]
1
0.8
0.6
0.4
0.2
0
P0
P10
100 nm
100 nm

Figure S3

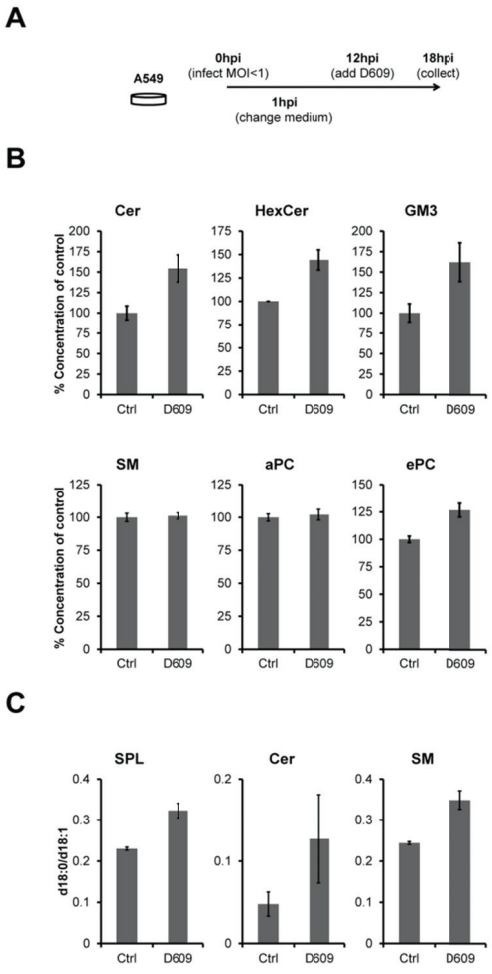
A
A549
0hpi
(infect MOI<1)
1hpi
(change medium)
12hpi
(add D609)
18hpi
(collect)
B
Cer
HexCer
GM3
SM
aPC
ePC
% Concentration of control
Ctrl
D609
C
SPL
Cer
SM
d18:0/d18:1

Figure S4

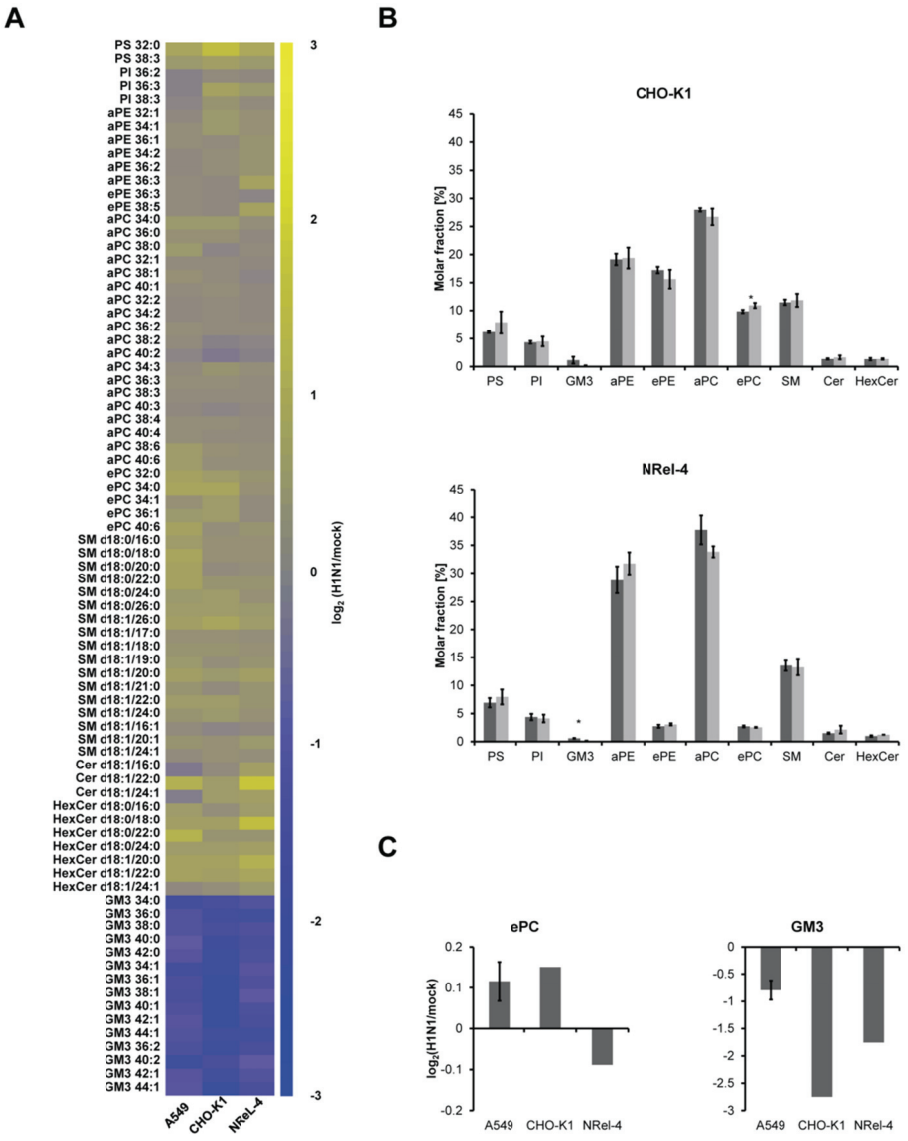
A
PS 32:0
PS 38:3
PI 36:2
PI 36:3
PI 38:3
aPE 32:1
aPE 34:1
aPE 36:1
aPE 34:2
aPE 36:2
aPE 36:3
ePE 36:3
ePE 38:5
aPC 34:0
aPC 36:0
aPC 38:0
aPC 32:1
aPC 38:1
aPC 40:1
aPC 32:2
aPC 34:2
aPC 36:2
aPC 38:2
aPC 40:2
aPC 34:3
aPC 36:3
aPC 38:3
aPC 40:3
aPC 38:4
aPC 40:4
aPC 38:6
aPC 40:6
ePC 32:0
ePC 34:0
ePC 34:1
ePC 36:1
ePC 40:6
SM d18:0/16:0
SM d18:0/18:0
SM d18:0/20:0
SM d18:0/22:0
SM d18:0/24:0
SM d18:0/26:0
SM d18:1/26:0
SM d18:1/17:0
SM d18:1/18:0
SM d18:1/19:0
SM d18:1/20:0
SM d18:1/21:0
SM d18:1/22:0
SM d18:1/24:0
SM d18:1/16:1
SM d18:1/20:1
SM d18:1/24:1
Cer d18:1/16:0
Cer d18:1/22:0
Cer d18:1/24:1
HexCer d18:0/16:0
HexCer d18:0/18:0
HexCer d18:0/22:0
HexCer d18:0/24:0
HexCer d18:1/20:0
HexCer d18:1/22:0
HexCer d18:1/24:1
GM3 34:0
GM3 36:0
GM3 38:0
GM3 40:0
GM3 42:0
GM3 34:1
GM3 36:1
GM3 38:1
GM3 40:1
GM3 42:1
GM3 44:1
GM3 36:2
GM3 40:2
GM3 42:1
GM3 44:1
A549
CHO-K1
NRel-4
3
2
1
0
-1
-2
-3
log2 (H1N1/mock)
B
CHO-K1
Molar fraction [%]
PS PI GM3 aPE ePE aPC ePC SM Cer HexCer
NRel-4
Molar fraction [%]
PS PI GM3 aPE ePE aPC ePC SM Cer HexCer
C
ePC
log2(H1N1/mock)
A549 CHO-K1 NRel-4
GM3
A549 CHO-K1 NRel-4

Figure S5

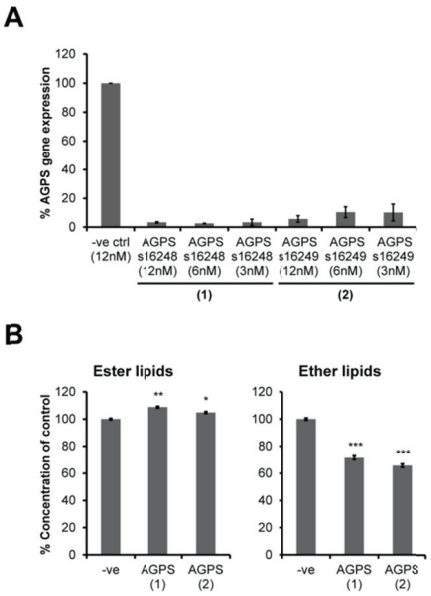
A
% AGPS gene expression
120
100
80
60
40
20
0
-ve ctrl (12nM)
AGPS s16248 (12nM)
AGPS s16248 (6nM)
AGPS s16248 (3nM)
AGPS s16249 (12nM)
AGPS s16249 (6nM)
AGPS s16249 (3nM)
(1)
(2)
B
Ester lipids
Ether lipids
% Concentration of control
**
*
***
***
-ve
AGPS (1)
AGPS (2)

Figure S6

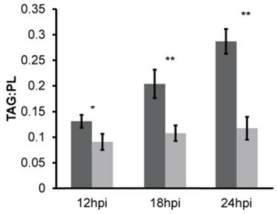

Figure S7